Lab on a Chip

An in vitro tumor swamp model of heterogeneous cellular and chemotherapeutic landscapes

Journal:	*Lab on a Chip*
Manuscript ID	LC-ART-02-2020-000131.R1
Article Type:	Paper
Date Submitted by the Author:	19-May-2020

Complete List of Authors:	Lin, Ke-chih; Princeton University, Department of Electrical Engineering Sun, Yusha; Princeton University, Department of Physics Torga, Gonzalo; Johns Hopkins Medical Institutions Campus, Urology Sherpa, Pema; Princeton University, Department of Physics zhao, yihua; Shenzhen University Qu, Junle; Shenzhen University, Institute of Optoelectronics Amend, Sarah; Johns Hopkins Medical Institutions Campus, Urology Pienta, Kenneth; Johns Hopkins Medicine Sturm, James C; Princeton University (PRISM), Department of Electrical Engineering Austin, Robert; Princeton University, Department of Physics

Cite this: DOI: 00.0000/xxxxxxxxxx

An in vitro tumor swamp model of heterogeneous cellular and chemotherapeutic landscapes

Ke-Chih Lin[1,*], Yusha Sun[1,*], Gonzalo Torga[2], Pema Sherpa[1], Yihua Zhao[3], Junle Qu[3], Sarah Amend[2], Kenneth J. Pienta[2], James C. Sturm[1], Robert H. Austin[1]

Received Date
Accepted Date

DOI: 00.0000/xxxxxxxxxx

The heterogenous, highly metabolic stressed, poorly irrigated, solid tumor microenvironment – the tumor swamp – is widely recognized to play an important role in cancer progression as well as the development of therapeutic resistance. It is thus important to create realistic *in vitro* models within the therapeutic pipeline that can recapitulate the fundamental stress features of the tumor swamp. Here we describe a microfluidic system which generates a chemical gradient within connected microenvironments achieved through a static diffusion mechanism rather than active pumping. We show that the gradient can be stably maintained for over a week. Due to the accessibility and simplicity of the experimental platform, the system allows not only well-controlled continuous studies of the interaction among various cell types at single-cell resolution, but also parallel experimentation for time-resolved downstream cellular assays on the scale of weeks. This approach allows for simple, compact implementation and is compatible with existing 6-well imaging technology for simultaneous experiments. As a proof-of-concept, we report the co-culture of a human bone marrow stromal cell line and a bone-metastatic prostate cancer cell line using the presented device, revealing on the same chip a transition in cancer cell survival as a function of drug concentration on the population level while exhibiting an enrichment of poly-aneuploid cancer cells (PACCs) as an evolutionary consequence of high stress. The device allows for the quantitative study of cancer cell dynamics by real-time monitoring of the interactions of various cell types with considerable experimental throughput.

1 Introduction

Aggressively growing solid tumors rapidly outstrip the ability of the circulatory system to develop a coherent microcirulatory network around the tumor[1], resulting in cancer cells within the tumor far from the characteristic diffusion length of $\approx 200\ \mu$m for resources within normal tissue[2]. This results in the generation of the internal "tumor" swamp, a region of the tumor with extreme metabolic stress[3]. There is also clear evidence of extensive interaction between cancer cells and other cancer cells, host stromal cells and cancer cells, as well as cancer-influenced host cells (e.g. cancer-associated fibroblasts, myofibroblasts, and macrophages) with other host cells within the tumor microenvironment[4]. The microenvironment is characterized by a profound heterogeneity in the distribution of chemotherapy, oxygen, or other resources[5,6]. Thus, solid tumors are better described within an ecological framework in which diffusion is the primary transporter of metabolites and chemotherapy, not the active hydrodynamic flow of normally irrigated tissue. In the context of a passive environment that applies strong selective pressure, the swamp presents opportunities for genetic or epigenetic changes crucial for cancer cell survival in environments where normal cells cannot survive.

Dynamics among various cell types within the tumor microenvironment have also been shown to affect the phenotypic behavior of cancer cells. These different cells also exist within the swamp. Traditional well-mixed cell culture provides a homogeneous environment that does not take into account the spatial complexities within a tumor swamp. Further, *in vivo* mouse models often lack the temporal resolution necessary to observe cellular processes[7]. Thus, more representative *ex vivo* models are required to recreate the adaptive tumor microenvironment in which cancer resides. Recent efforts have explored the potential for such models to develop patient-specific treatments[8].

An intuitive way of generating diffusive heterogeneity *in vitro* is to induce a purely diffusive chemical gradient within an artificial microenvironment, as chemical gradients typically hold a key role in regulating a number of cellular functions *in vivo* including migration, proliferation, differentiation, and carcinogenesis. Microfluidic devices have become a versatile platform for precise gradient control[9,10]. These gradient-generating devices can be broadly categorized into (i) constant flow generators which provide fixed boundary conditions[11–13], and (ii) static generators which are solely based on diffusion[14–16].

As illustrated in Fig. 1a, constant flow generators require an active pressure source to drive the media and create laminar flow in order to establish stable and time-independent chemical gradients within the microfluidic channels. Most of the existing flow-based gradient generators are associated with significant hydrodynamic shear stresses, which cause disruption of cell proliferation and affect cell morphology through various flow-mediated mechanisms such as mechanotransduction[17]. In contrast, as shown in Fig. 1b,

*These authors contributed equally to this work.
[1]*Department of Physics, Princeton University, Princeton, NJ*
[2]*Johns Hopkins Medical Institute, Baltimore, MD*
[3]*College of Physics, Shenzhen University, Shenzhen, China*

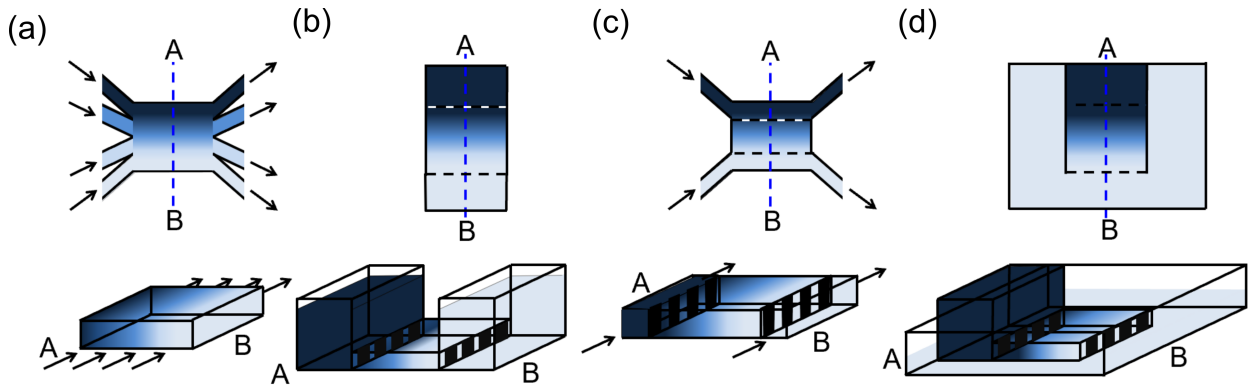

Fig. 1 **Schematic diagrams of major microfluidic gradient generation mechanisms (top view and isometric view).** (a) Constant flow gradient generators provide exceptional control over gradient precision and time efficiency. The hydrodynamic flow, however, leads to disruption of cell culture. For all diagrams, "A" and "B" denote opposing maximum and minimum chemical concentrations, as visualized by the shades of blue. (b) Static gradient generator with open-ended reservoirs offer a more desirable environment for cell growth, but are more suitable for short-term experiment since media replenishment could disrupt the distribution of chemical concentration. (c) Gradient generation through combination of laminar flow and diffusion resolves the issues as seen in (a) and (b). Nevertheless, the experimental setup could be complicated and labor-intensive. (d) A simplified schematic figure of the static gradient generator presented in this paper. With one enclosed reservoir and one open-ended reservoir, media in the outer buffer can be replenished without disturbing the chemical gradient. Long-term experiments can be performed without complicated tubing connections and bulky peripheral equipment for an active media source.

static gradient generators establish a gradient without the presence of advection flow, offering a much more desirable physical environment for cell growth. However, static gradient generators require frequent media replenishment, which usually disrupts the distribution of chemical concentration through the period of an experiment.

Several attempts have been made to combine the advantages of flow-based devices and static gradient generators [18–22]. As shown in Fig. 1c, the media flowing channels and cell culture chambers are separated by slits which greatly increase the fluidic resistance and prevent shear stresses across cell culture chamber. As a result, long-term experiments can be done in the scale of several weeks. However, the application of these devices as pre-clinical research platforms remains limited, as the experimental setup is a complicated and labor-intensive process. Further, the need of active pressure source such as a syringe-pump limits the experiment throughput.

Based on the philosophy of Sewall Wright, if a population of cells is split into a *metapopulation* and allowed to interact on a fitness landscape, the evolutionary dynamics of the system can be rapidly accelerated. From this principle, we have shown previously that these metapopulations, or weakly connected microenvironments, within a microfluidic device may induce rapid emergence of bacterial resistance to antibiotics as well as the formation of poly-aneuploid cancer cells (PACCs) in the context of chemotherapeutic resistance [23–25]. However, the previously reported microfluidic devices are designed based on gradient generation mechanism demonstrated in Fig. 1c, which restricts the scalability of the experimentation platform.

In this paper, we describe a microfluidic device that constructs cancer cell metapopulations on a stress landscape yet does not require syringe pumps as active media sources as in [21,25]. The presented device, the static evolutionary accelerator (EA), generates a stable chemical gradient through diffusion between an on-chip pre-filled reservoir and an outer media buffer. This design overcomes the major challenges we faced throughout the development of the technology by successfully transitioning from a flow-based to a passive diffusion approach for gradient generation across the microhabitat array, enabling our ability to conduct long-term experiments with a much simpler, cost-effective, and seamless experimental setup in an effort to expand the use of microfluidic devices in preclinical cancer research.

As illustrated in Fig. 1d, the design of the chip allows the media in the outer buffer to be replenished without disturbing the chemical gradient. This is achieved since one of the reservoir is enclosed and filled up with fluid, such that the variation of fluid level in the outer open-ended reservoir caused by media replenishment does not induce fluid advection. Without otherwise bulky peripheral equipment for an active media source, the experimental setup is greatly simplified and allows for high-throughput experimentation. Multiple experiments can be easily performed simultaneously, enabling numerous potential applications including but not limited to parallel experimentation for time-resolved downstream cellular assays, high-throughput drug screening, *ex vivo* modeling and predictions for patient-specific treatments.

We validated the stability of the drug gradient within the static EA via COMSOL Multiphysics simulation and a physical gradient test with a fluorescent dye. We further cultured a bone metastatic prostate cancer cell line with an epithelial phenotype (PC3-EPI) with a human bone marrow stromal cell line (HS-5) using the presented microfluidic static EA and observed cancer cell propagation for 6 days in the presence of a gradient of the chemotherapeutic docetaxel. This device has potential therapeutic implications as a robust *in vitro* platform for a wide-variety of preclinical studies that better depict the human tumor microenvironment.

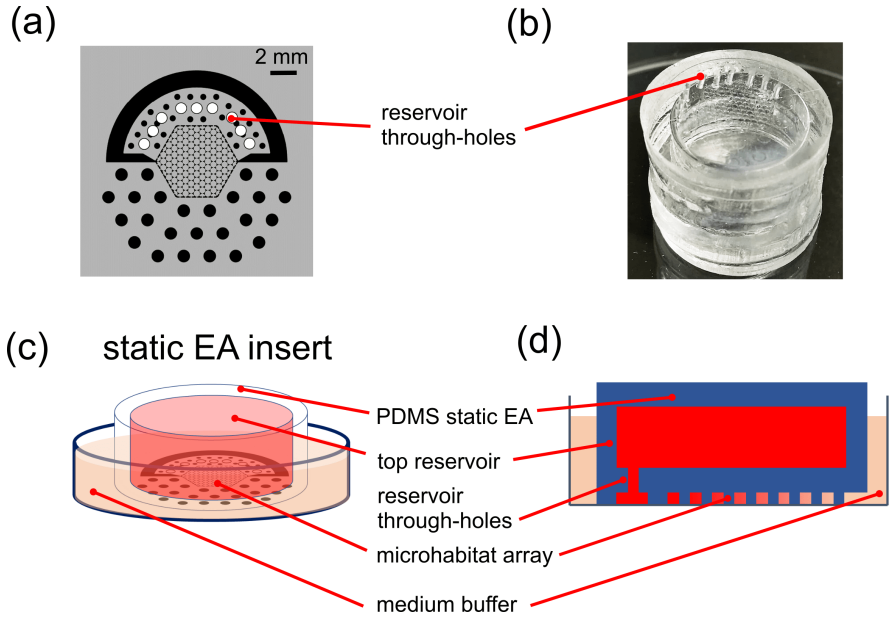

Fig. 2 **Design and implementation of the static evolutionary accelerator (EA) insert.** (a) Schematic design of hexagonal microhabitat array to be etched onto a silicon wafer for a depth of 100 μm. White circles with the design indicate punched through-holes connecting the microhabitat array to the on-chip media reservoir. Dark structures within the scheme illustrate the PDMS-casted walls that enclose the cells and support the device. Each side of each hexagonal microhabitat is 350 μm and the diameter of the entire chip is 21 mm. (b) Components of the PDMS-based static EA insert in practice. From top to bottom: micro-structured layer, capping layer, reservoir, and another capping layer. The microstructured layer is generated from soft lithography based on the silicon wafer patterned with the structure in (a). (c — d) Illustration of how gradients are generated from tilted side view and cross-section perspectives. The media in the top reservoir (red) and in the medium buffer (orange) contain varying concentrations of the reagents of interest. Reagents diffuse across the hexagonal microhabitat array and generate 2D gradients within the cell culture region. The combination of the PDMS chip and the outer cell culture vessel is called an "static EA insert," which is placed in a customized sample holder described in Fig. 3.

2 Experimental

2.1 Microfluidic chip design and fabrication.

The microfluidic device pattern consists of hexagonal microenvironments, in which cells can be cultured (Fig. 2a). The device consisting of the pattern on the bottom and a reservoir to hold cell medium can be adhered to a 2-dimensional surface of cells (Fig. 2b, c). Cell medium that has drug can be filled on the outside, such that diffusion occurs inwards in one direction along the chip and also outwards from the reservoir (Fig. 2d). Diffusion fluxes between the source with no drug and the source with drug can balance, setting up a gradient of drug. Note that the operation of gradient generation can be reversed; i.e., the media in the outer region may contain reagent of interest while the media in the top reservoir contains normal growth media. Because there is no additional opening in the top reservoir, regardless of the height of outer buffer media level, there is no fluid advection in the device.

Specifically, the microfluidic device, made of polydimethylsiloxane (PDMS), consists of two compartments: the on-chip medium reservoir and a PDMS microstructured chip with 109 interconnected hexagonal and 24 half-hexagonal chambers (Fig. 2a). The hexagonal chambers are 350 μm in side length. The floor of the lowest level of the PDMS device upon which the cells move is a 35mm diameter hydrophilic 20-micron thick Lumox^{TM} gas permeable film (Sarstedt, D 51588 Nmbrecht, Germany). Chemicals diffuse into the hexagonal chambers through the 15-micron wide and 180-micron long slits between the periphery channels and the hexagonal array. In order to create the device, a silicon wafer is fabricated using standard photolithography (using light to pattern a thin film), deep reactive-ion etching (for 100 μm etch depth), and silanization. The PDMS (Sylgard 184 silicone elastomer kit) is mixed and poured onto the silicon wafer, degassed in a vacuum chamber, and further cured overnight at 70° C. Afterwards, the PDMS chip is peeled from the wafer and through-holes are punched through the PDMS allow fluid flow. The PDMS chip is then bonded with a reservoir and capping layer of PDMS (Fig. 2b) via oxygen plasma treatment. For gradient experiments (Fig. 5), black food coloring was added to the uncured PDMS to dissociate background fluorescence effects.

2.2 Cell culture platform and assembly.

A stainless steel 6-well plate was designed to hold up to 6 Lumox^{TM} dishes as well as 6 devices (Fig. 3a). Each static EA insert includes an opening for media replenishment, the top of which is covered by microadhesive sealer. The 6-well plate has double layer 35 mm glass windows underneath each Lumox^{TM} dish to maintain thermal isolation and prevent water condensation. The plate can be set up during experiments lasting up to several weeks with suitable environmental factors such as an Ibidi thermal control unit that keeps the cells at 37° C and a custom gas supply that mixes ambient air with the desired 5% CO_2. The gas supply system connects to the dish and pressurizes the Lumox^{TM} membrane against the chip, ensuring sealing of the chip and the formation of the hexagonal microenvironments (Fig. 3b). The flow of normoxia gas can be regulated by gas valves and the gauge

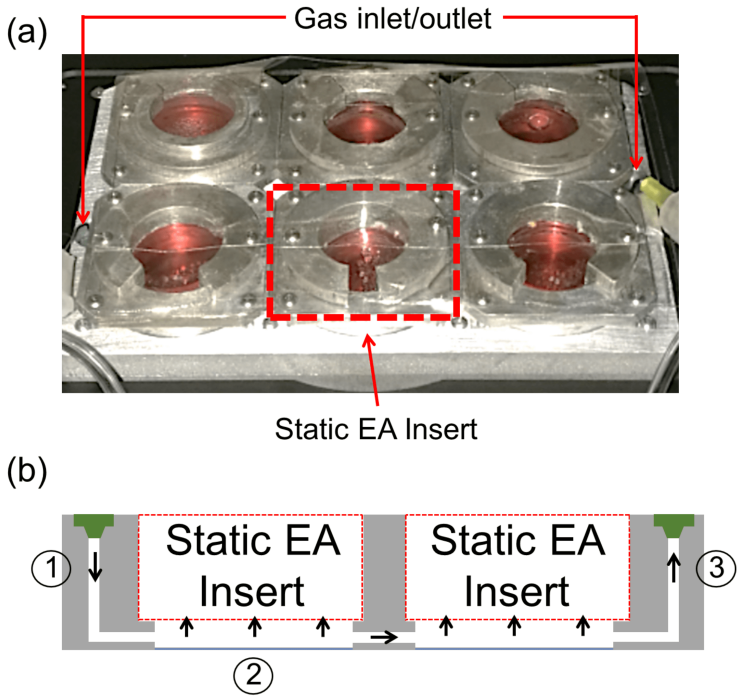

Fig. 3 **Customizable setup allowing for long-term parallel experimentation.** (a) Components of a six-well plate designed to hold up to six microfluidic chips to achieve parallelization. The solid red arrows indicate ports for gas supply influx and efflux, which uniformly pressurizes the chips. A static EA insert is indicated with a dotted red arrow. (b) Schematic of experimental setup, whereby the six-well plate including microfluidic chips is placed within an Ibidi incubator that regulates temperature (37° C) and humidity (90%). The gas supply that pressurizes the Lumox^{TM} dishes and seals the microfluidic chips is set to 5% CO_2, 20% O_2, and 75% N_2 and flows in through the port labeled 1, underneath the static EA inserts labeled 2, then out through a port labeled 3.

pressure is typically maintained at around 0.2 psi (1.4×10^4 Pa). The pieces of the six-well plate can be cleaned and reused by a standard solid autoclave procedure.

2.3 Device operation.

24 hours prior to the start of experimentation, the desired cell lines are detached with 0.05% trypsin/EDTA (Sigma-Aldrich) and pelleted. A total of 5×10^4 cells are cultured in each Lumox^{TM} dish on the six-well plate. Cells are allowed to adhere in an incubator. 3 hours before the beginning of the experiment, the PDMS devices are disinfected via UV exposure for $15-20$ minutes and treated in an oxygen plasma system for around 30 seconds to create hydrophilicity at the microstructure layer. Immediately afterwards, pre-warmed culture medium at 37° C, degassed in a vacuum chamber for 5 minutes, is injected into the on-chip reservoirs via 22-gauge syringes. The degassing procedure of the media minimizes chances for entrapment of microbubbles within the structures on the chip. Note that this procedure sets up a gradient with the high drug region on the outside of the chip; alternatively, injected pre-warmed medium with drug reverses the gradient.

To initiate the experiment, the medium within the Lumox^{TM} dishes (with cells adhered) is replaced by 1 mL of prewarmed and degassed medium. Chips are then placed directly on top of the gas-permeable Lumox^{TM} membranes by approaching the surface at a 15° angle to minimize bubble formation. Each chip is then clamped into place onto the culture dish and a sheet of microadhesive sealer is spread over the top of the PDMS chip to minimize medium evaporation. The entire six-well plate is placed into an on-stage incubator on the motorized stage of an inverted epifluorescence microscope. The gas supply pressurizes the Lumox^{TM} membranes against the PDMS chip to ensure sealing of the device. Medium with drug can be replenished every 2 days by extracting or injecting 1 mL directly through the microadhesive sealer from or into the area surrounding the PDMS chip. The reagent of interest then diffuses into the hexagonal cell culture region, setting up a gradient with the normal culture medium diffusing out through the through-holes on the reservoir.

2.4 Data acquisition and image processing.

To generate population data with sufficient temporal resolution, we utilized in this paper time-lapse image acquisition on an inverted epifluorescence microscope with a motorized x-y stage, focus knob, shutter, and filter cubes. Fluorescence images may also be taken manually at desired time points. In our experiments, we employed the Nikon NIS-Elements software to acquire stitched images across various channels at 10x magnification with autofocus routines. Images were taken every hour, with experiments possessing the ability to run on the time scale of weeks.

After the experiment, images were converted to TIFF format and compressed (Fiji/ImageJ software). Fluorescence intensities were quantified via ImageJ and relevant algorithms such as background subtraction and particle analysis to determine cell number

were performed (Supplementary Material). MATLAB ver. R2019a and Graphpad Prism 8.3.0 were employed for graphical output.

3 Results and discussion

3.1 Demonstration of gradient generation.

We modeled the process of gradient formation numerically via the diffusion equation with fixed boundary conditions (COMSOL Multiphysics). The COMSOL simulation demonstrates the distribution of reagent concentration (Fig. 4a) and magnitude of diffusion flux (Fig. 4b) in the static EA at steady state, with the diffusion coefficient set to be 10^{-9} m^2/s and boundary conditions of 0 nM and 10 nM. We consider two scenarios: 1) the 10 nM reagent diffuses out from the top reservoir, into the hexagonal array, and then diluted at the open boundary at the bottom, and 2) the 10 nM reagent is added in the outer region, diffuses into the hexagonal array, then diluted by the on-chip reservoir. The results of these two cases (Fig. 4a — b and Fig. 4c — d) are symmetrical. The line profile of the diffusion flux magnitude around the circular outer boundary is plotted in Fig. 4e. The total loss of reagent is equal to the integral of the diffusion flux magnitude over the corresponding surface area, which gives the dissipation of the reagent per second as 4.4×10^{-19} mol/s. Note that the total amount of reagent in the reservoir or medium buffer is 2×10^{-11} mol, such that the dissipation of the reagent is negligible within the period of the experiment (Fig. 4f). Therefore, during the period of the experiment, we may assume the concentration of reagent stays constant on the boundary.

Compared with flow-driven gradient generators, this static diffusion mechanism requires a longer time to establish the concentration profile pattern. To measure the timescale of gradient generation and to validate the predictions of our simulations, we performed a gradient test with a fluorescent hydrophilic small-molecule organic dye, rhodamine-6G. The reservoir of the static EA was filled up with 0.1 mM rhodamine-6G. In order to block the background fluorescent signal from the rhodamine-6G within the reservoir, we employed a black PDMS chip by mixing black food-dye into the PDMS elastomer prior to the curing process. The gradient of fluorescence intensity, which is directly proportional to the concentration of rhodamine-6G, increased monotonically and reached equilibrium by 24 hours after chip installation (Fig. 5a,b). Four indicated areas on the chip show that a stable linear gradient is established through 8 days after the start of the experiment, once normalized for background light intensity (Fig. 5c,d).

We also investigated the diffusion of rhodamine-6G into PDMS as a potential source of error, as PDMS is known to absorb small chemical molecules[26,27]. In our case, we typically work with small, charged molecules which should not have high diffusion constants within a well-cured (24 hours at 60° C) PDMS polymer. However, to test this assumption, we measured the increase in fluorescent intensity of a sealed PDMS pillar over time (Fig. 6a). We can obtain a rough estimate of the upper bound of the diffusion coefficient of a charge dye (rhodamine 6G) through PDMS by considering the 1D diffusion equation

$$\frac{\partial c}{\partial t} = D\frac{\partial^2 c}{\partial x^2},$$

where intensity $I \sim c$. The pillar is around 760 μm in length and thus $\Delta x \approx 380$ μm. We take maximum fluctuations of around 100 units of intensity across the pillar, and employ 1 unit of intensity per day as $\frac{\partial c}{\partial t}$ by taking the standard error of the slope of the best-fit line to the linear portion of Fig. 6b. This calculation assumes all fluctuations in observed intensity across the pillar are attributed to diffusional effects and therefore correspond to an upper bound. We find that diffusion effects of the dye into the PDMS is negligible after controlling for background noise, with an calculated upper bound for the diffusion coefficient of rhodamine-6G into PDMS as $1.7 \cdot 10^{-10}$ cm^2/s, a very small number compared to the diffusion of the dye in water, which is on the order of 10^{-5} cm^2/s (Fig. 6c, d). Therefore, we do not believe that small molecule diffusion through PDMS significantly influences the static gradient. Notably, the lack of active source (pump) guarantees bubble-free and static fluid dynamics, which ensures stable chemical gradient across the chip. This pump-free configuration is compatible with commercial-sized well plates and allows for much higher experiment throughput. The aforementioned advantages allow the cell culture device to be an ideal platform to investigate the population dynamics of cancer cells in a chemotherapy-induced stress landscape.

3.2 Population dynamics of bone marrow stroma and cancer cells.

To determine the capability of the device to provide suitable conditions for cellular propagation under a chemotherapeutic gradient over long time scales, PC3-EPI, a E-cadherin/CDH1-positive/vimentin-negative PC3 clone with epithelial phenotype described previously[25], was co-cultured with HS5, a human bone marrow fibroblast stromal cell line (ATCC). PC3-EPI were engineered via lentiviral vector to possess nuclear histone fluorescence with green fluorescent protein (GFP) and constitutive cytoplasmic fluorescence with mCherry[25]. Docetaxel was used to generate linear gradients of 0 to 15 nM across the static EA. Employing the platform as described in Fig. 3, we performed 6 simultaneous experiments that included gradient verification, no gradient, and varying gradient conditions (Supplementary Fig. 1). Real-time imaging of cells were conducted with three different channels, brightfield, mCherry, and GFP, across the entirety of each static EA at 10x magnification every hour. Images were stitched together in the NISElements software, and analysis was conducted after importing to ImageJ/Fiji software. Image processing and cell counting were achieved with a custom protocol and set of algorithms (Supplementary Fig. 2). Movies of relevant gradient and control experiments are provided in Supplementary Material.

We describe a representative experiment in Fig. 7, which shows the progression of PC3-EPI cancer cells and HS5 stromal cells within the static EA chips under the conditions of either no docetaxel present or a 15 nM gradient of docetaxel, with cancer cell

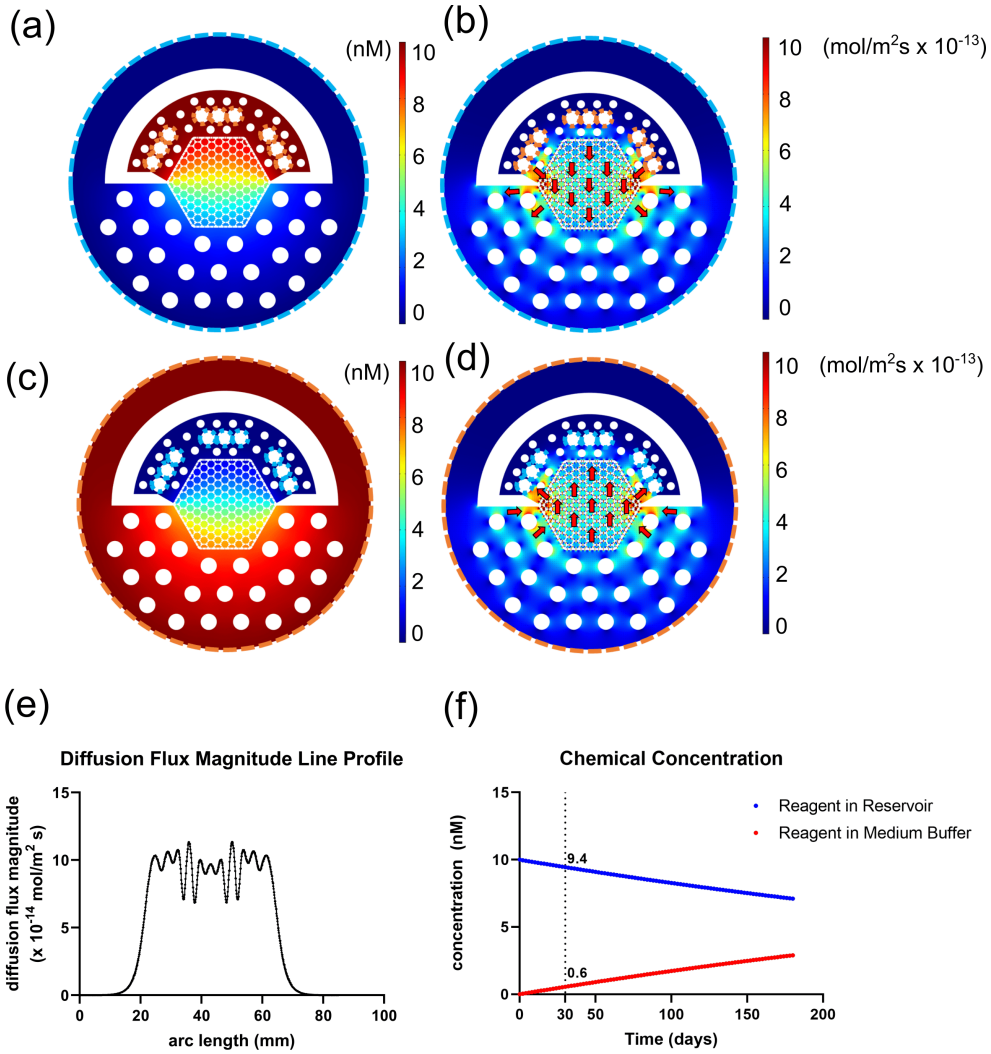

Fig. 4 **COMSOL Multiphysics® simulation of the static diffusion mechanism and theoretically predicted gradients in microfluidic device.** (a) Simulated reagent concentration distributions across the chip in the case where reagent diffuses outwards from the on-chip reservoir. Reagent diffuses from the nine circular through-holes at the top of the chip, into the hexagonal array, then diluted through the open boundary at the bottom of the array. Boundary conditions were set as 10 nM at the through-holes and 0 nM at the open boundary. (b) Magnitude of diffusion flux in the same simulation as in (a), with red arrows indicating direction of diffusion. The diffusion coefficient was set to be 10^{-9} m^2/s. (c) Simulated reagent concentrations across the chip with reagent diffusing inwards from the outer region, with normal media in the on-chip reservoir. Boundary conditions were set as 0 nM at the through-holes and 10 nM at the open boundary. (d) Magnitude of diffusion flux in the same simulation as in (c), with red arrows indicating direction of diffusion. The diffusion coefficient was set to be 10^{-9} m^2/s. (e) Line profile of diffusion flux magnitude around the entirety of the chip boundary. (f) Concentration of reagent over time depending on where the reagent is located. Within 30 days, the concentration of the reagent in either the reservoir or the medium changes by around 6%, which is robust enough for practical experimental purposes.

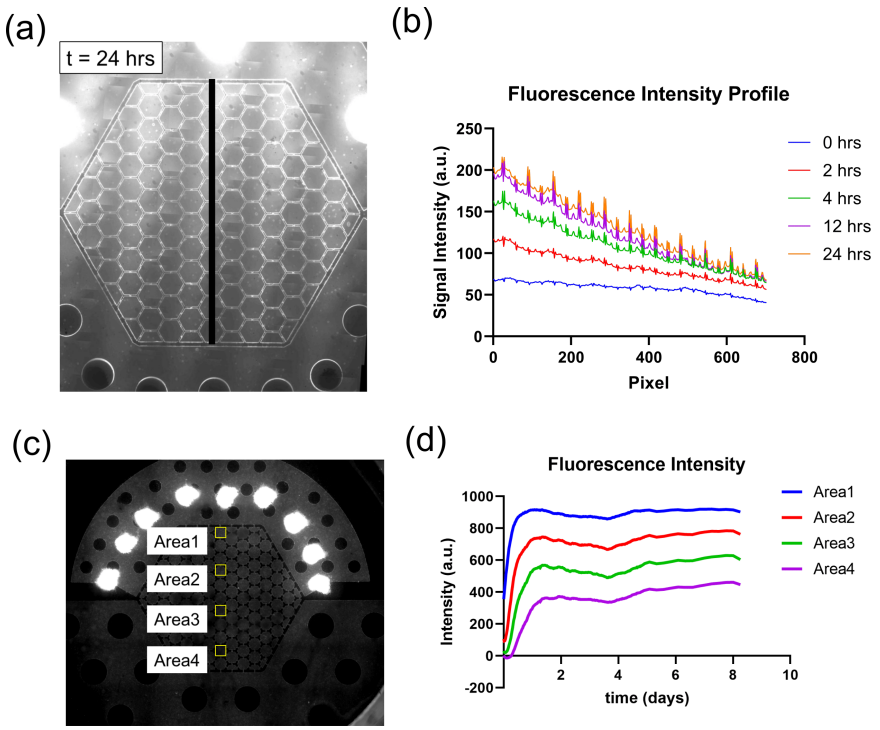

Fig. 5 **Verification of gradient generation across multiple days.** (a) A static EA with reservoir filled with 0.1 mM of rhodamine6G, a fluorescent dye, at $t = 24$ hours post-installation. The marked black line indicates the fluorescence intensity line profile measured vertically across the chip. (b) Line profiles of fluorescence intensity as shown across the chip in (a) at various time points. The gradient stabilizes at around 24 hours. Peaks in the profile reflect uneven changes in the intensity as the border of a microhabitat is crossed. (c) Observation of four indicated areas on the static EA, with reservoir filled with rhodamine6G dye. (d) Longitudinal time profile of the four areas in (c) across 8 days, indicating that intensity and corresponding gradient remain stable across the device and across time.

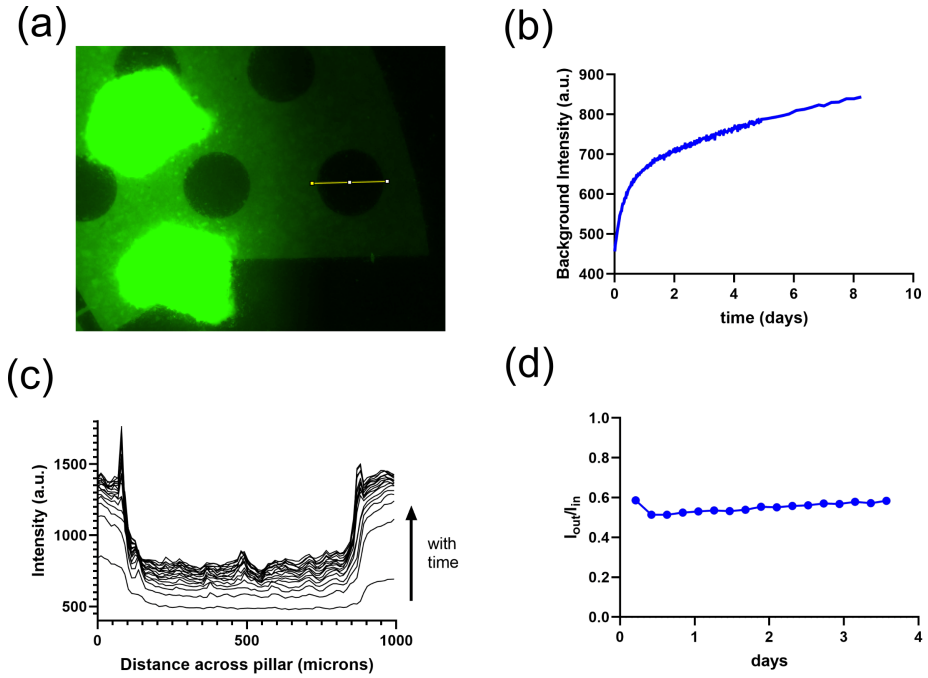

Fig. 6 **Insignificant contribution of diffusion of dye through PDMS.** (a) Analysis is focused on the pillar on PDMS indicated with a yellow line. This pillar is sealed to the Lumox^{TM} membrane with dye occupying the space surrounding the pillar. (b) Increase in the intensity of the center of the pillar over the course of an 8-day experiment. (c) Line profile of the pillar in part (a) over time. The curves generally reveal a uniform profile within the pillar at any particular point in time, with the average intensity increasing quickly then leveling off. Since there is always a uniform profile within the pillar, there are negligible diffusional effects. (d) Ratio of the intensity outside the pillar I_{out} (first point in each profile in part (c)) to the average intensity within the pillar I_{in} over time. The ratio is relatively conserved through time, implying that general increases in intensity are background noise effects and do not affect I_{out} or I_{in} in varying ways.

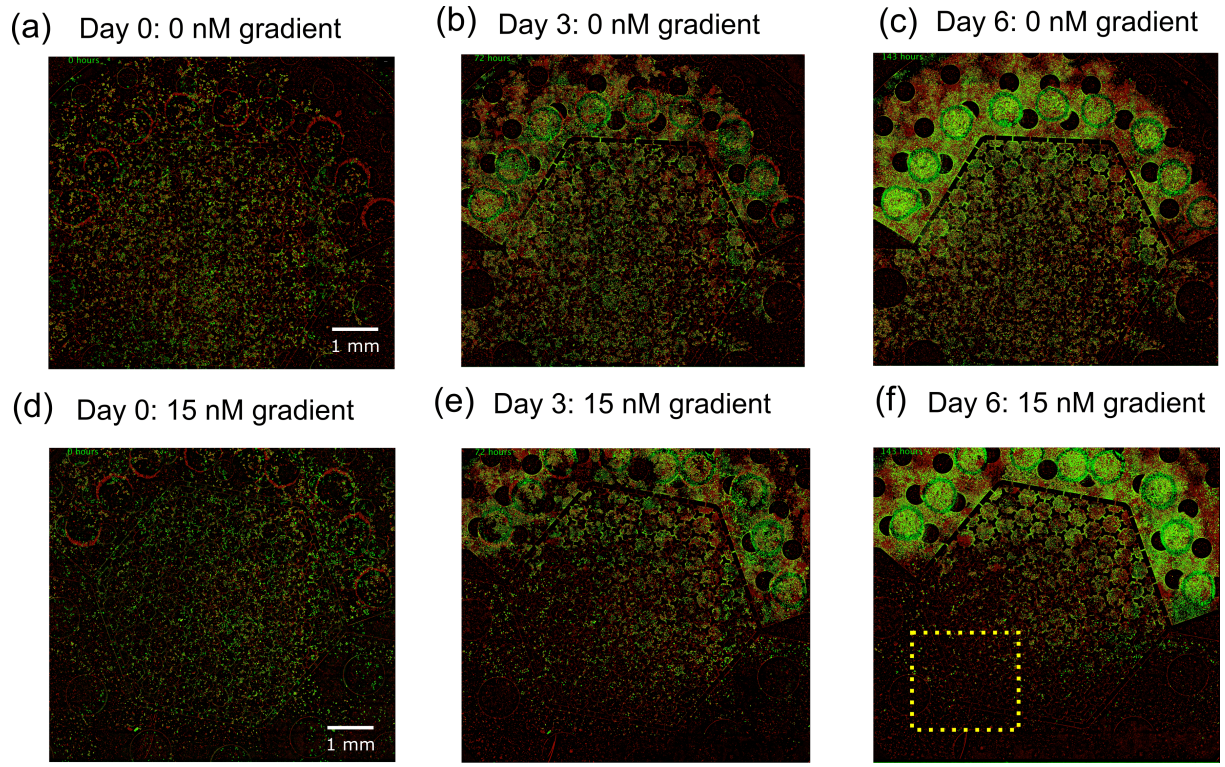

Fig. 7 **Visualization of proof-of-principle coculture of PC3-EPI (nuclear GFP stain, colored as green) and HS-5 (processed brightfield, colored as red) without drug and with docetaxel gradient (0 to 15 nM).** (a — c) Co-culture of PC3-EPI and HS-5 without drug in a control experiment, with images shown on days 0, 3, and 6. The scale bar shown in (a) applies to both (b) and (c). PC3-EPI cells achieved confluency by day 3. (d — f) Co-culture of PC3-EPI and HS-5 with docetaxel in a gradient ranging from 15 nM (outside region) to 0 nM (on-chip reservoir), at days 0, 3, and 6. The scale bar shown in (d) applies to both (e) and (f).

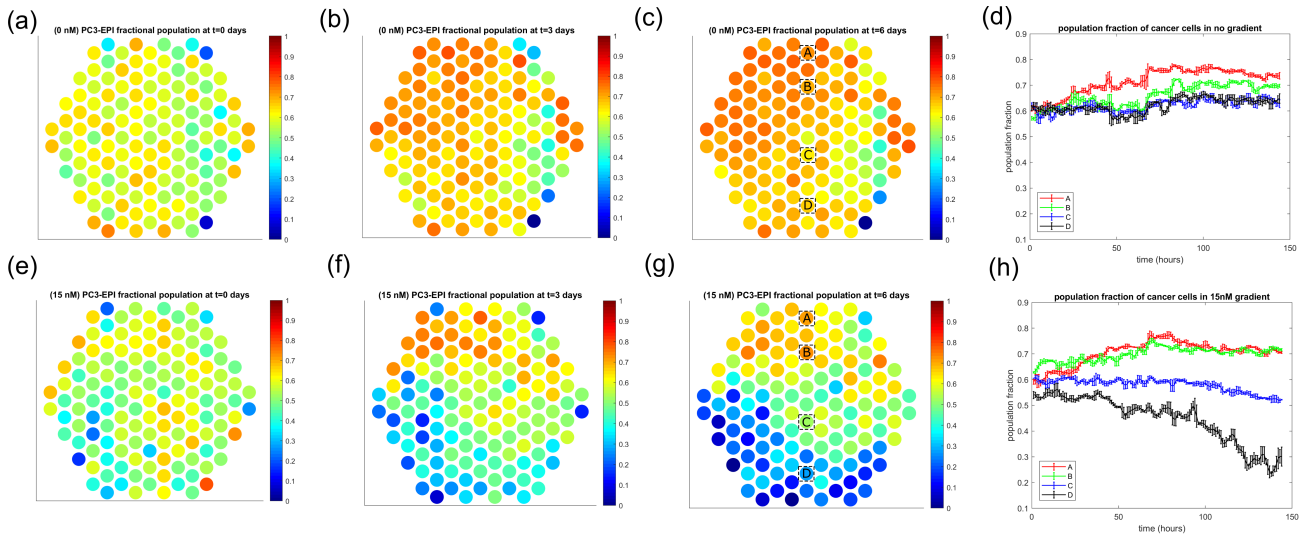

Fig. 8 **Population spatial distribution of cancer PC3-EPI for control and gradient experiments.** (a) Analysis performed on images such as those shown in Fig. 7 to determine the population fraction of cancer cells in a control experiment with no drug gradient at $t = 0$ days. The population fraction is charted as a heatmap within the hexagonal array, with each circle corresponding to a microhabitat in the static EA. Each colored dot follows the range depicted in the color bar to the right representing the average PC3-EPI fractional population calculated for each representative time point for both the drug gradient (15 nM) and control (0 nM) experimental series. (b) Similar plot as in (a) but at $t = 3$ days. (c) Similar plot as in (a) but at $t = 6$ days. (d) Time evolution of cancer population fraction for the control experiment across four distinct areas of the EA chip (A, B, C, D as shown in (c)). Data are displayed as a moving mean with $n = 3$. Error bars correspond to the mean $\pm$ moving standard deviation of adjacent 3 data points. (e) Population fraction of cancer cells in a representative experiment with a 15 nM docetaxel gradient at $t = 0$ days. The drug gradient is established from the bottom of the chip (high-drug area) to the top of the chip (low-drug area). (f) Similar plot as in (e) but at $t = 3$ days. (g) Similar plot as in (f) but at $t = 6$ days. (h) Time evolution of cancer population fraction for 15 nM gradient experiment at the same areas of the EA chip (A, B, C, D as shown in (g)), where data are displayed with moving mean ($n = 3$) $\pm$ moving standard deviation ($n = 3$).

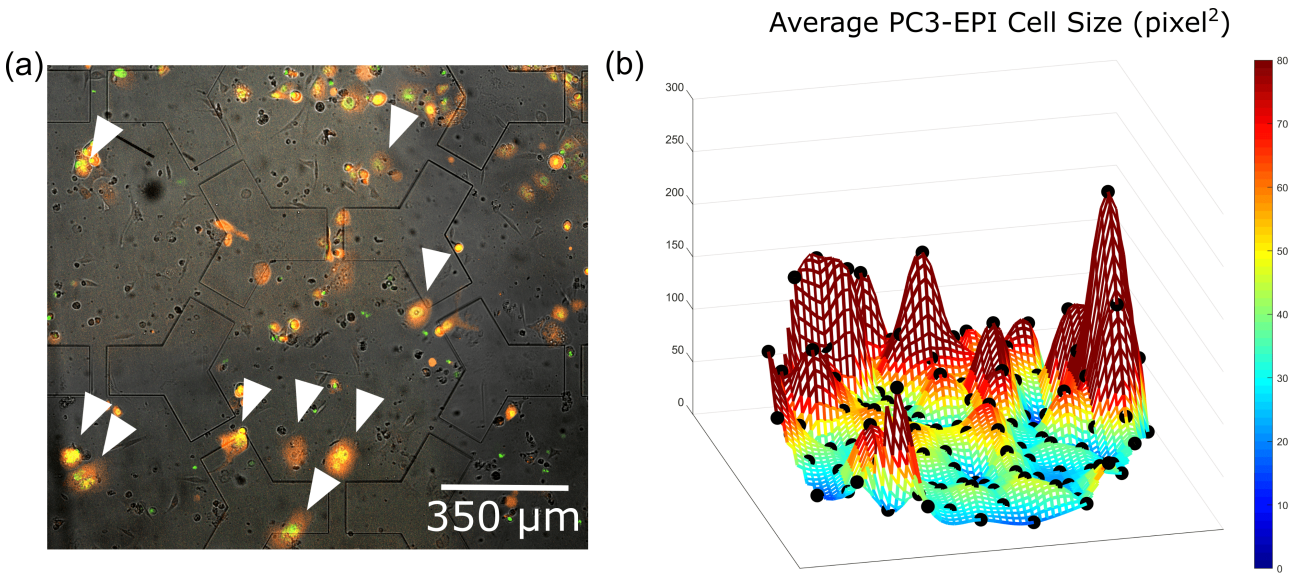

Fig. 9 **Exemplification of evolutionary phenomenon of emergence of poly-aneuploid cancer cells (PACCs) in high-stress areas.** (a) PACCs are indicated with white arrows. Brightfield, red, and green channels overlay capturing non-labeled stromal cells only visible in pure brightfield and PC3-EPI fluorescently-labeled nuclear and cytoplasmic cellular components of each cell displayed respectively in the red and green channels. Image taken from boxed region from Fig. 7f for Day 6 within the 15 nM gradient. (b) Average PC3 cell size per microhabitat across the chip for Day 6 populations as in Fig. 8g based on percentage area coverage by cancer cell cytoplasm.

nuclei colored as green (GFP fluorescence) and stromal cells colored red (processed brightfield). The gradient is established with the high-drug region at the bottom of the chip (Fig. 7c,d). To better understand these dynamics, we quantified these cell count data and demonstrate population behavior in Fig. 8. In particular, we describe the cancer population proportion p_γ, defined as

$$p_\gamma = \frac{\gamma}{\gamma + s},$$

where γ and s are the cell counts for PC3-EPI and HS5, respectively. In the control condition without docetaxel, PC3-EPI cancer cells grew homogenously across the microhabitats to reach high confluence by 3 days (Fig. 8a — d, Supplementary Fig. 3), with the time scale of growth comparable to previous experiments with pump-driven devices[21]. However, within the 15 nM gradient experiment, with an originally relatively uniform populations of both cancer and stromal cells, by day 3, a marked transition in cancer cell population fraction occurs, revealing differential effects of docetaxel as a function of drug concentration (Fig. 8e—h, Supplementary Fig. 3). The continuous transition in population dominance of cancer cells is maintained and magnified through 6 days of experimentation (Fig. 8g). The population fractions plotted in Fig. 8d, h correspond to the time course of particular microhabitats denoted in Fig. 8c, g. The curves for both Fig. 8d, h are relatively smooth, and the gradual transition from growth to failure to survive suggests that, locally, the drug concentration has a monotonically increasing negative effect on cancer cell proliferation. The observation of the transition in cancer fractional population dominance was similarly noted across separate experiments (Supplementary Movies).

Notably, whereas on the population level, cancer cells fail to survive in high-drug areas, we observe that among the cancer cells that do survive, many of the cells consistently surviving in areas of high stress exhibit an enrichment of the poly-aneuploid phenotype with enlarged cell size and either an enlarged nucleus or multiple nuclei (Fig. 9a), corroborating the results of Lin *et al.* (2019)[25]. Accordingly, the average cell size per microhabitat increases across the chip within the 15 nM gradient experiment at 6 days, suggesting an enrichment of these cells at higher drug concentration under the assumption that phenotypically larger cells correlate with a poly-aneuploidy subpopulation (Fig. 9b). Studies have reported previously the association between higher DNA content ($> 4n$) and cell volume, both in the context of eukaryotic cells in general and in cancer[28–30]. In particular, we have previously shown that large size and polyploidy are key defining features of PACCs and have demonstrated that when PACCs are formed, either by fusion or failed cytokinesis, that their size is increased[25,31]. Future study will focus on the mechanism of evolution of these resistant cells, their characterization via downstream analysis, and the potential role of stroma in mediating resistance.

4 Conclusions

In this paper, we have designed a static microfluidic-based cancer-on-chip device with the ability to generate stable and controlled gradients of chemotherapy across connected microenvironments. This system presents a novel static gradient generation method, alleviating the need for pump-driven flow-based methods, significantly reducing experimental workload and increasing throughput. We modeled computationally the formation of a two-dimensional gradient on the time scale of weeks and validated

the ability for the microfluidic static EA to maintain this gradient utilizing fluorescent dyes.

There is a need for more representative *in vitro* models to reproduce the tumor microenvironment prior to animal models in the drug development pipeline in order for a better prediction of cancer progression as well as responses to drugs within dynamical stress landscapes. Within these local environments, for example, the cooperative interaction between tumor cells and the surrounding environment has been characterized as survival strategies against drugs[32,33]. Specifically, prostate cancer is well-known for predominantly metastasizing into bone marrow. The bone marrow provides an environment for metastasized prostate cancer, allowing the cancer cells to stay dormant for a period of time before transitioning into the proliferating phase[34,35]. The process of how and why prostate cancer can be triggered to exit dormancy state and proceed to subsequent secondary tumor growth remains poorly understood.

Our evolutionary accelerator (EA) device offers a robust, high-throughput method to recapitulate elements of the complex *in vivo* microenvironment by allowing for multiple cell types to interact on a fitness landscape, driven by faster evolution in a low-N limit of isolated but connected populations. In comparison to other platforms to probe the roles of tumor-stroma interactions in chemotherapeutic resistance[36], we demonstrate the implications of population heterogeneity to cellular response to a drug gradient, recapitulating the drug-induced evolutionary stress within the tumor microenvironment through chemotherapy. We have previously shown, for example, that in such systems with weakly connected microhabitats, cells that become stress-resistant or mutants in one area can migrate to areas of even higher stress since they will possess greater fitness relative to other cells[25]. Furthermore, since the total number of cells is greatly decreased in areas of higher stress, the mutants can more easily establish themselves within that new habitat[25].

As a proof-of-principle demonstration of our microfluidic system, we studied the co-culture of PC3-EPI prostate cancer cells with HS5 human bone marrow cells under a gradient of docetaxel. We employed extended time-lapse imaging on an on-stage incubator with high spatial and temporal resolution. We find a continuous transition in cancer cell proliferation and survival across the same chip on a population level, both in terms of raw cell count and relative fractional population when compared to the stromal cells. We further observe the emergence of large poly-aneuploid cancer cells at high-drug regions on the chip as a consequence of drug-induced genomic instability. We note that, within our technology, nutrient content within media diffuses uniformly throughout the hexagonal microhabitat array in theory; nevertheless, more validation needs to be conducted to ensure that cellular dynamics are not affected by local metabolite depletion within the microenvironments. If necessary, channel sizes could be modulated accordingly. Further, the precision of stromal cell automated counting faces limitations due to the nonuniformity of brightfield imaging but can be alleviated by employing fluorescently labeled stromal cell lines. Further work will involve downstream sequencing analysis of resistant subpopulations and explore the role of cell migration within the evolutionary dynamics.

This device will be important to future studies on the complex interactions between multiple cell types in a heterogeneous micro-ecological stress landscape. We hope that this work will act as a more robust preclinical platform for drug development and contribute to better understanding of how issues such as drug heterogeneity may have implications for tuning of chemotherapy scheduling, drug resistance, or recurrence.

Conflicts of interest

There are no conflicts to declare.

Acknowledgements

This work was supported by NSF PHY-1659940 and the Princeton Catalysis Initiative. YS was supported by the SURE Program of the James Buchanan Brady Urological Institute at Johns Hopkins School of Medicine for a part of this research.

Author Contributions

Conceptualization: KL, YS, JC, KP, JQ, RA. Formal Analysis: YS, KL. Investigation: KL, YS, GT, KM, PS, YZ, RA. Software: KL, YS. Supervision: JC, RA. Resources: SA, KP. Methodology: KL, YS, RA. Writing - original draft: YS, KL, RA. Writing - review & editing: YS, KL, RA. All authors read and approved the final draft.

Notes and references

1 Vasan, N., Baselga, J. & Hyman, D.M. (2019). A view on drug resistance in cancer. Nature 575, 299–309.

2 Grimes, D. R., Kelly, C., Bloch, K., & Partridge, M. (2014). A method for estimating the oxygen consumption rate in multicellular tumour spheroids. Journal of The Royal Society Interface, 11(92), 20131124.

3 Amend, S. R., & Pienta, K. J. (2015). Ecology meets cancer biology: the cancer swamp promotes the lethal cancer phenotype. Oncotarget, 6(12), 9669.

4 Whiteside, T. L. (2008). The tumor microenvironment and its role in promoting tumor growth. Oncogene, 27(45), 5904.

5 Tannock, I. F., Lee, C. M., Tunggal, J. K., Cowan, D. S., & Egorin, M. J. (2002). Limited penetration of anticancer drugs through tumor tissue: a potential cause of resistance of solid tumors to chemotherapy. Clinical cancer research, 8(3), 878-884.

6 McGranahan, N., & Swanton, C. (2017). Clonal heterogeneity and tumor evolution: past, present, and the future. Cell, 168(4), 613-628.

7 Sontheimer-Phelps, A., Hassell, B. A., & Ingber, D. E. (2019). Modelling cancer in microfluidic human organs-on-chips. Nature Reviews Cancer, 1.

8 Yi, H. G., Jeong, Y. H., Kim, Y., Choi, Y. J., Moon, H. E., Park, S. H., ... & Paek, S. H. (2019). A bioprinted human-glioblastoma-on-a-chip for the identification of patient-specific responses to chemoradiotherapy. Nat. Biomed. Eng, 1(1).

9 Tsai, H. F., Trubelja, A., Shen, A. Q., & Bao, G. (2017). Tumour-on-a-chip: microfluidic models of tumour morphology, growth

and microenvironment. Journal of the Royal Society Interface, 14(131), 20170137.

10 Keenan, T. M., & Folch, A. (2008). Biomolecular gradients in cell culture systems. Lab on a Chip, 8(1), 34-57.

11 Jeon, N. L., Dertinger, S. K., Chiu, D. T., Choi, I. S., Stroock, A. D., & Whitesides, G. M. (2000). Generation of solution and surface gradients using microfluidic systems. Langmuir, 16(22), 8311-8316.

12 Cimetta, E., Cannizzaro, C., James, R., Biechele, T., Moon, R. T., Elvassore, N., & Vunjak-Novakovic, G. (2010). Microfluidic device generating stable concentration gradients for long term cell culture: application to Wnt3a regulation of β-catenin signaling. Lab on a chip, 10(23), 3277-3283.

13 Zhang, Y., Xiao, R. R., Yin, T., Zou, W., Tang, Y., Ding, J., & Yang, J. (2015). Generation of gradients on a microfluidic device: toward a high-throughput investigation of spermatozoa chemotaxis. PloS one, 10(11), e0142555.

14 Diao, J., Young, L., Kim, S., Fogarty, E. A., Heilman, S. M., Zhou, P., ... & DeLisa, M. P. (2006). A three-channel microfluidic device for generating static linear gradients and its application to the quantitative analysis of bacterial chemotaxis. Lab on a Chip, 6(3), 381-388.

15 Abhyankar, V. V., Toepke, M. W., Cortesio, C. L., Lokuta, M. A., Huttenlocher, A., & Beebe, D. J. (2008). A platform for assessing chemotactic migration within a spatiotemporally defined 3D microenvironment. Lab on a Chip, 8(9), 1507-1515.

16 Kim, D., Lokuta, M. A., Huttenlocher, A., & Beebe, D. J. (2009). Selective and tunable gradient device for cell culture and chemotaxis study. Lab on a Chip, 9(12), 1797-1800.

17 Davies, P. F., Barbee, K. A., Volin, M. V., Robotewskyj, A., Chen, J., Joseph, L., ... & DePaola, N. (1997). Spatial relationships in early signaling events of flow-mediated endothelial mechanotransduction. Annual review of physiology, 59(1), 527-549.

18 Wu, A., Loutherback, K., Lambert, G., Estévez-Salmerón, L., Tlsty, T. D., Austin, R. H., & Sturm, J. C. (2013). Cell motility and drug gradients in the emergence of resistance to chemotherapy. Proceedings of the National Academy of Sciences, 110(40), 16103-16108.

19 Wu, A., Zhang, Q., Lambert, G., Khin, Z., Gatenby, R. A., Kim, H. J., ... & Austin, R. H. (2015). Ancient hot and cold genes and chemotherapy resistance emergence. Proceedings of the National Academy of Sciences, 112(33), 10467-10472.

20 Han, J., Jun, Y., Kim, S. H., Hoang, H. H., Jung, Y., Kim, S., ... & Park, S. (2016). Rapid emergence and mechanisms of resistance by U87 glioblastoma cells to doxorubicin in an in vitro tumor microfluidic ecology. Proceedings of the National Academy of Sciences, 113(50), 14283-14288.

21 Lin, K. C., Torga, G., Wu, A., Rabinowitz, J. D., Murray, W. J., Sturm, J. C., ... & Austin, R. (2017). Epithelial and mesenchymal prostate cancer cell population dynamics on a complex drug landscape. Convergent science physical oncology, 3(4), 045001.

22 Lin, K. C., Torga, G., Sun, Y., Pienta, K. J., Sturm, J. C., & Austin, R. H. (2019). Generation of Heterogeneous Drug Gradients Across Cancer Populations on a Microfluidic Evolution Accelerator for Real-Time Observation. Journal of visualized experiments: JoVE, (151).

23 Lambert, G., Estévez-Salmeron, L., Oh, S., Liao, D., Emerson, B. M., Tlsty, T. D., & Austin, R. H. (2011). An analogy between the evolution of drug resistance in bacterial communities and malignant tissues. Nature Reviews Cancer, 11(5), 375.

24 Zhang, Q., Lambert, G., Liao, D., Kim, H., Robin, K., Tung, C. K., ... & Austin, R. H. (2011). Acceleration of emergence of bacterial antibiotic resistance in connected microenvironments. Science, 333(6050), 1764-1767.

25 Lin, K. C., Torga, G., Sun, Y., Axelrod, R., Pienta, K. J., Sturm, J. C., & Austin, R. H. (2019). The role of heterogeneous environment and docetaxel gradient in the emergence of polyploid, mesenchymal and resistant prostate cancer cells. Clinical & experimental metastasis, 1-12.

26 Toepke, M. W., & Beebe, D. J. (2006). PDMS absorption of small molecules and consequences in microfluidic applications. Lab on a Chip, 6(12), 1484-1486.

27 Goudie M.J., Ghuman A.P., Collins S.B., Pidaparti R.M., & Handa H. (2016) Investigation of Diffusion Characteristics through Microfluidic Channels for Passive Drug Delivery Applications. J Drug Deliv. doi:10.1155/2016/7913616

28 Coward, J., & Harding, A. (2014). Size does matter: why polyploid tumor cells are critical drug targets in the war on cancer. Frontiers in oncology, 4, 123.

29 Mirzayans, R., Andrais, B., & Murray, D. (2018). Roles of polyploid/multinucleated giant cancer cells in metastasis and disease relapse following anticancer treatment. Cancers, 10(4), 118.

30 Zhang, S., Mercado-Uribe, I., Xing, Z., Sun, B., Kuang, J., & Liu, J. (2014). Generation of cancer stem-like cells through the formation of polyploid giant cancer cells. Oncogene, 33(1), 116-128.

31 Amend, S. R., Torga, G., Lin, K. C., Kostecka, L. G., de Marzo, A., Austin, R. H., & Pienta, K. J. (2019). Polyploid giant cancer cells: Unrecognized actuators of tumorigenesis, metastasis, and resistance. The Prostate, 79(13), 1489-1497.

32 Meads, M. B., Gatenby, R. A., & Dalton, W. S. (2009). Environment-mediated drug resistance: a major contributor to minimal residual disease. Nature reviews cancer, 9(9), 665.

33 Valkenburg, K. C., de Groot, A. E., & Pienta, K. J. (2018). Targeting the tumour stroma to improve cancer therapy. Nature reviews Clinical oncology, 15(6), 366.

34 Park, S. H., Keller, E. T., & Shiozawa, Y. (2018). Bone marrow microenvironment as a regulator and therapeutic target for prostate cancer bone metastasis. Calcified tissue international, 102(2), 152-162.

35 Morrissey, C., & Vessella, R. L. (2007). The role of tumor microenvironment in prostate cancer bone metastasis. Journal of cellular biochemistry, 101(4), 873-886.

36 McMillin, D. W., Delmore, J., Weisberg, E., Negri, J. M., Geer, D. C., Klippel, S., ... & Griffin, J. D. (2010). Tumor cell-specific bioluminescence platform to identify stroma-induced changes

to anticancer drug activity. Nature medicine, 16(4), 483.

20-word sentence of text highlighting novelty of work: **A microfluidic platform was developed that generates a gradient of chemotherapy via diffusion to study evolutionary dynamics of cancer.**